Wind Tunnel Measurement of the Urban Wind Field for Flight Path Planning of Unmanned Aerial Vehicles

Jürgen Frey *, Hannes Rienecker†, Sebastian Schubert‡, Veit Hildebrand§ and Harald Pfifer ¶
Technische Universität Dresden, 01307 Dresden, Germany

The focus of the present paper is the investigation of the wind field along the flight path of a small fixed-wing unmanned aerial vehicle (UAV) in an urban environment. The considered mission is a goods delivery as part of a last-mile logistics system. A representative downtown environment of a typical European city is studied. As was recently shown, the local wind field between the buildings can be exploited to obtain energy optimal flight paths for a UAV. So far these results are solely based on numerical simulations. In this paper, the numerical simulations of the wind field are supplemented and verified by wind tunnel experiments. For the wind tunnel tests a 1:100-scale model of the benchmark environment is used. Velocity profiles are measured with hot-wire probes and a five-hole pneumatic probe at several positions along the flight path. The latter is used to detect the flow direction. A combination of aerodynamic alignment and multi-zone approach for calibration is used to determine the local wind vectors. Further attention is paid to the turbulence and gustiness of the local flow. The present work constitutes an important step in the evaluation of the exploitation potential of local wind effects on UAV flight path planning.

I. Introduction

The last-mile logistics representing the final link in a supply chain, is distinguished by its short distance, but is often also the most inefficient section. The use of small UAV, both fixed-wing and rotary, for last-mile logistics in an urban environment has been under discussion throughout the last years. These vehicles operate autonomously and are not affected by traffic jams. However, range and payload of electrically powered UAV are still quite limited [1]. Therefore, economically reasonable operation of delivery drones requires a high energy efficiency, as the battery size directly affects payload capacity and range. Due to the low cruise speeds of small UAV, their performance is strongly influenced by the atmospheric wind field. In urban environments this wind field is greatly affected by the buildings and therefore of complex structure. For this reason, adapting the flight path to the wind conditions offers great potential to save energy, increase range and/or payload, respectively.

As part of the German Federal Ministry for Economic Affairs and Climate Action funded project URBANSens, the TU Dresden's Chair of Flight Mechanics and Control studies exactly this energy saving potential by optimizing UAV flight paths in urban environments based on the knowledge of the local wind field. Initial results of the flight path optimization already highlight the potential of the approach, see [2–4]. All results are obtained for a generic city model as proposed in [2], which can be called representative for a typical central European urban area. In all references, the wind field of a reference urban environment has been obtained numerically with help of the Large-Eddy-Simulation (LES) tool PALM [5]. LES can capture unsteady flow phenomena such as gusts and turbulence. Using turbulence models, this kind of simulation enables comparatively coarse grids and thus significantly less computing power than direct numerical simulation. Still, it has to be emphasized that flow fields between buildings are highly complex consisting of unsteady areas, interacting vortices and large backwater areas. As such, it is critical to validate the numerical results by experiments in order to gain more confidence in the optimized flight paths.

This paper contributes such a validation of the numerical results obtained in PALM by wind tunnel experiments in TU Dresden's low speed wind tunnel, see Section III. In a first step, the airflow between the buildings is studied qualitatively on a large scale by oil-flow-visualization supplemented by pressure probes in the ground, see Section IV.B. While the method provides a big picture of the flow field in the whole city model, it only considers flow close to the

*Research Assistant, Chair of Flight Mechanics and Control, juergen.frey@tu-dresden.de
†Research Assistant, Chair of Flight Mechanics and Control, hannes.rienecker@tu-dresden.de
‡Research Assistant, Chair of Flight Mechanics and Control, sebastian.schubert@tu-dresden.de
§Research Associate, Chair of Flight Mechanics and Control, veit.hildebrand@tu-dresden.de
¶Professor, Chair of Flight Mechanics and Control, harald.pfifer@tu-dresden.de

surface. Hence, additional discrete quantitative measurements using hot wire and a five-hole probe to obtain mean velocity and wind direction, respectively, are presented in Section IV.C. The measurement points are chosen based on the energy optimal flight path from a scenario in [3]. The mean wind speed and wind direction is compared to the LES results.

II. Modelling the Wind Field within an Urban Environment Using LES

To develop and test a novel approach for determining energy-optimal flight trajectories in an urban wind field, a reference city model was created in [2]. This model represents a typical arrangement of eight buildings found in central European urban areas. The topography includes three 50-meter-high residential buildings in the west, four 20-meter-high terraced houses in the east, and a single 15-meter-high supermarket with an integrated office building in the north. Hence, it is a suitable benchmark to provide realistic wind conditions for UAV operations in urban environments.

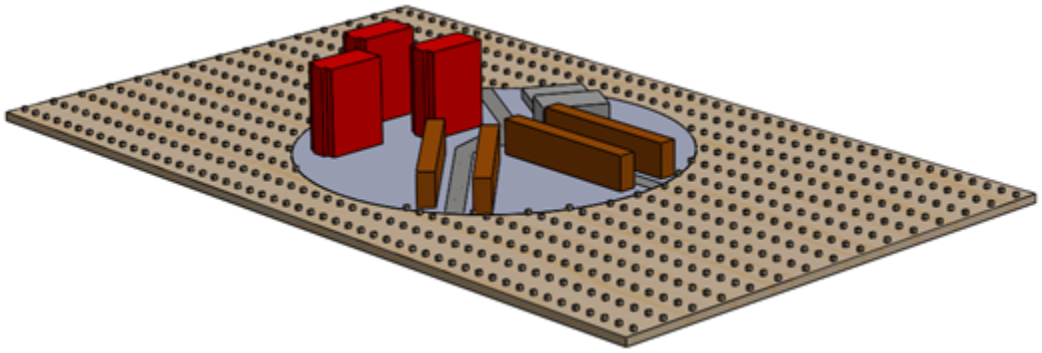

Fig. 1 Generic city model representing a typical central European urban area

Large-Eddy Simulations (LES) were conducted to determine the wind field within this reference area to provide wind field data for flight path optimization in a parallel work [2, 3]. The present paper focuses on validating the LES results obtained via the tool PALM [5] through wind tunnel experiments. To ensure comparable results, particular emphasis was placed on the LES inflow conditions. Notably, PALM generates velocity profiles and turbulence within the mean flow by cyclically applying the outflow conditions as an inflow boundary until the simulation converges to a final state. In order to expedite convergence, appropriate starting conditions, such as a reasonable velocity profile, were selected. In this case, the wind profile obtained from a previous wind tunnel experiment was used in [2, 3] to initialize the simulation. This profile is based on guidelines of environmental aerodynamics according to the VDI standard [6]. Moreover, an obstacle-free extended computational domain is essential in the vertical, lateral, and flow directions to capture all pertinent flow phenomena, such as the redevelopment of flow behind the wake region or the mitigation of acceleration resulting from contraction. The model adheres to guidelines outlined in [7] for distances from built-up areas to boundaries, ensuring robust CFD simulation of flows in the urban environment. PALM uses equidistant horizontal grid spacings, where each grid volume is designated as either air or solid, representing a building. The rectangular grid structure requires special attention when modelling oblique building walls. If more than half of a grid volume geometrically pertains to a building, the entire volume is assigned as a solid. A uniform grid size of $\Delta x, y, z$ =2.5 m was chosen for all experiments, offering an optimal balance between computational efficiency and accurate resolution of flow effects. Prior to using the data for trajectory optimization, it is necessary to confirm the full development of the LES. The time series analysis of kinetic energy, turbulent kinetic energy, and maximum velocity components demonstrates no trends anymore after approximately 4 hours of simulation time, indicating convergence in the simulation.

A reference task was chosen within the city model, as highlighted in Fig. 2. The objective was to minimize the energy required of the UAV to fly from Point South to Point North by taking advantage of local wind effects. The wind direction was consistently set from the west, considering the wake generated by the three high-rise buildings to represent an essential component of scenarios the UAV will experience in urban environments. Based on the numerical simulation results and flight path optimization methods developed within the project, a specific flight path example for the UAV was obtained, as shown in Fig. 3. Along this path, five positions have been selected for detailed evaluation of the local flow conditions. To date, the approach is based solely on time-averaged wind data, neglecting the dynamic variations and turbulent characteristics of the wind field. To ensure the validity and consistency of the energy savings

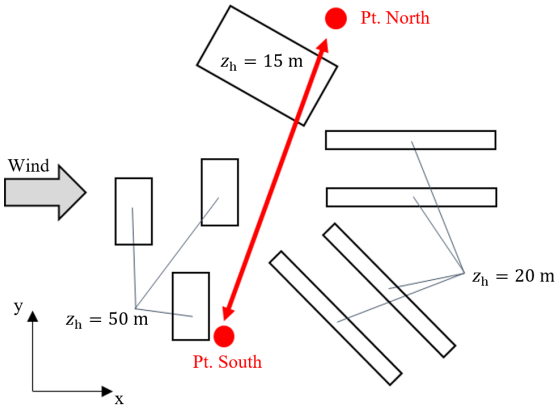

Fig. 2 Flight scenario for further study in the wind tunnel; the wind direction is considered constant from west

achieved, we focus on validating the LES results through wind tunnel experiments conducted along the flight paths. Detailed flow measurements are carried out and described in the subsequent sections. For additional information on the flight path optimization and further scenarios the reader is referred to [4].

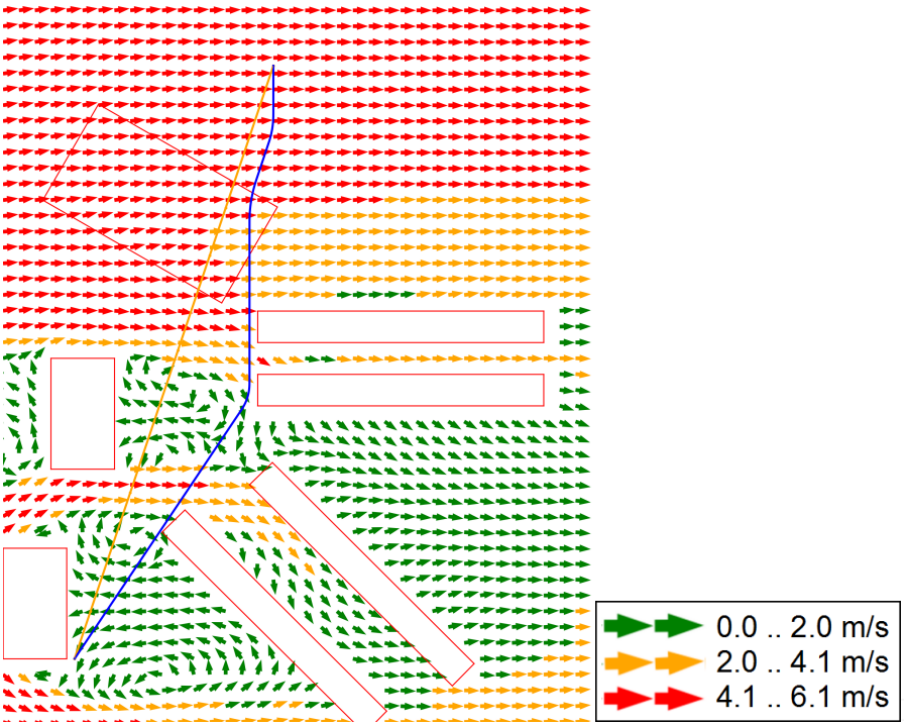

Fig. 3 Result of the LES-computation of the flow field with a wind speed u_{Ref}=6.5 m/s from the west including an optimized flight path from Point South to Point North [4].

III. Wind Tunnel Facilities and Experimental Setup

A. Low-Speed Wind Tunnel at TU Dresden

The Chair of Flight Mechanics and Control at TU Dresden operates a low-speed Göttingen-type wind tunnel with a closed circuit but an open test section, as depicted in Fig. 4. The tunnel has a circular nozzle with a 3-meter diameter and provides flow velocities of up to 40 m/s. Its contraction ratio is 7:1, leading to a free stream turbulence below 0.5%, which makes it suitable for conventional aeronautical applications. However, the wind field in lower regions of the atmosphere significantly differs from the low turbulence flow an aeroplane typically experiences. It is a highly unsteady boundary layer flow where gusts and turbulence are present at all length and time scales. Typical turbulence levels are about 30% (see [6] for details) in comparison to the 0.5% that TU Dresden's wind tunnel provides.

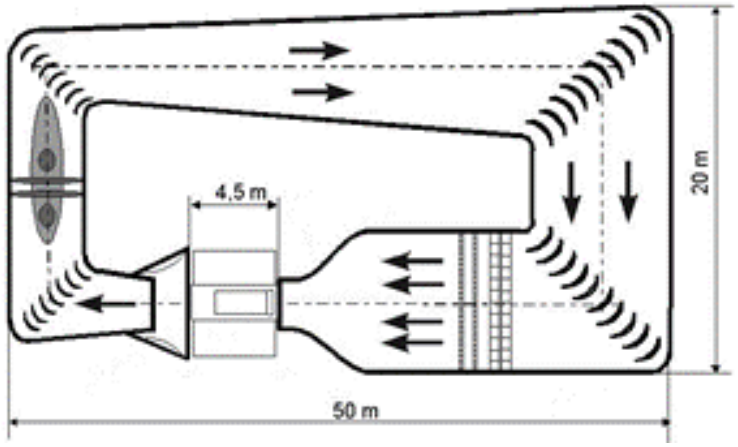

Fig. 4 Schematic of TU Dresden's wind tunnel.

For studying environmental aerodynamics in TU Dresden's wind tunnel, a turbulence grid is installed into the nozzle. Its purpose is shaping the velocity profile by its distributed blockage and, thus, generation of turbulence over the whole cross section. Additionally, roughness elements are installed on the floor to keep up the turbulence close to the ground. The setup is shown in Fig. 5.

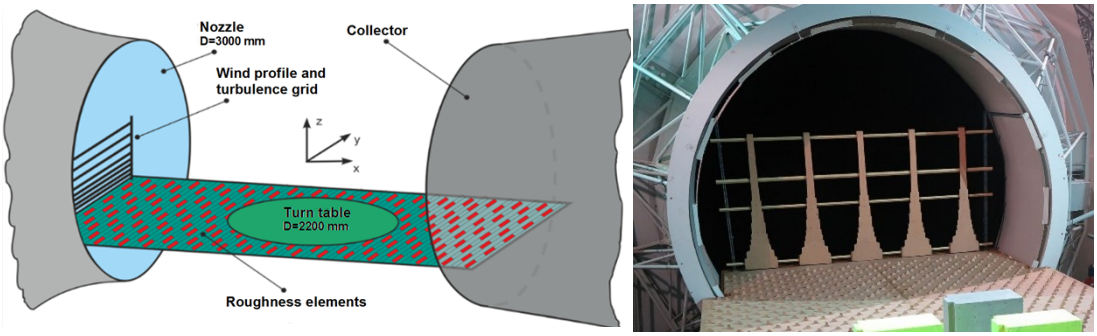

(a) Schematic of setup for environmental aerodynamics. **(b) Turbulence grid**

Fig. 5 Atmospheric boundary layer in TU Dresden's wind tunnel.

The city model used in the experiments is a 1:100-scale model of the reference city environment considered for the numerical simulation in PALM as described in Section II. Accordingly, it consists of three residential high-rise buildings (500 mm high), a low-rise building (150 mm high), and a four terraced houses (200 mm high). It is installed on a turntable (2.2 m diameter) within the test section, see Fig 6.

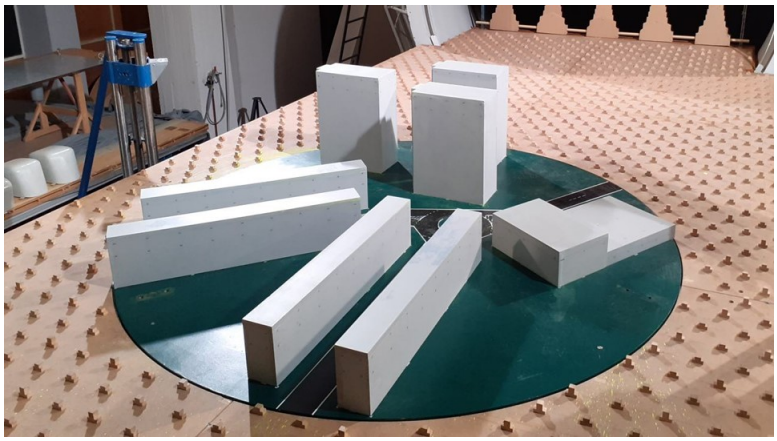

Fig. 6 Model of the urban area in the test section.

B. Experimental Setup

The experimental setup is shown in Fig. 7. Broadly speaking two series of experiments were conducted. In a first step, the flow close to the surface was studied. For this step oil-flow-visualization was used, as well as pressure probes flushed into the surface of the model. The positions of the latter are indicated by the black numbers in Fig. 7. In a second step, the wind profile was measured at five points, which were chosen along the considered flight path (green line in the figure). The points are denoted by underlined bold green numbers in Fig. 7. The wind profile measurements include hot wire probes to obtain the mean velocity profiles and a five-hole probe to measure the flow direction.

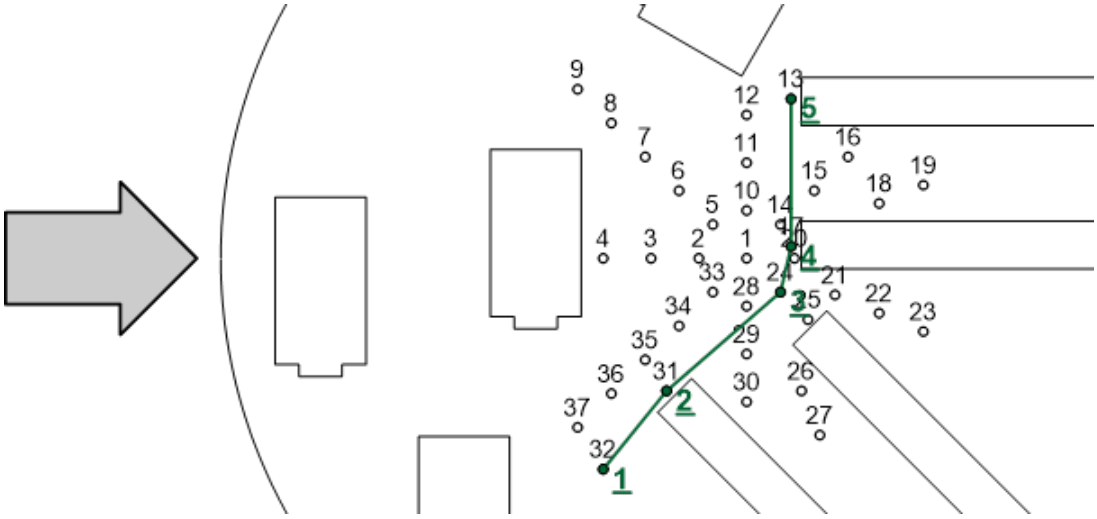

Fig. 7 Measurement positions in the experiment: small black numbers denote wall shear probes, whereas underlined bold green number denote the profile measurements along the considered flight path (green line).

1. Surface based measurements

Initially, oil-flow-visualization was applied on the model to show the wall stream lines on the floor and buildings. With this technique typical structures in the flow are identified, e.g., backwater areas and regions of high velocities where the flow is canalized and accelerated can be found. It is used mainly to spot areas of particular interest and informs the placement choice of quantitative measurement techniques. In addition to flow visualization, the near surface flow is studied by an arrangement of special pressure probes which are embedded into the model floor. The probes consist of simple pressure tubes protruding out of the floor by approximately 5 mm and ring-shaped orifices around its foot, see Fig. 8. The pressure difference between both orifices $\Delta c_p = \frac{p_1 - p_2}{q_\infty}$, where p_1 and p_2 are the pressure measurements as

depicted in Fig. 8 and q_∞ the dynamic pressure, is sensitive to the velocity gradient close to the ground and therefore the wall shear stress.

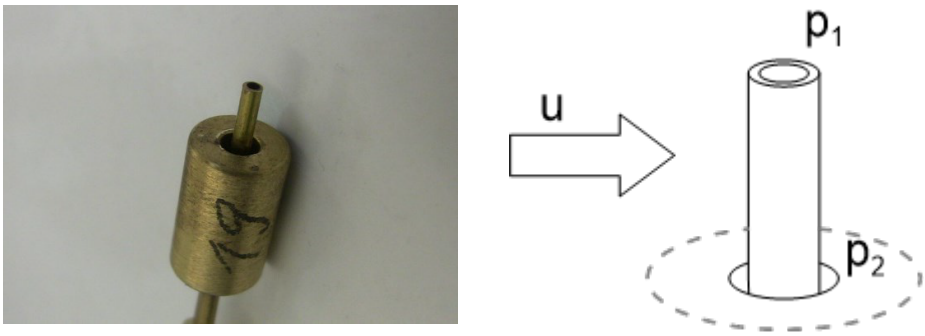

(a) Probe corpus **(b) Schematic view**

Fig. 8 Pressure probe for flush mounting in the ground.

2. Wind profile measurements

The hot wire anemometry used in the experiment is a standard constant-temperature-anemometer circuit. It has been calibrated according to King's law [8]. The probe has a vertically aligned wire making it sensitive to velocity components in the horizontal plane. It is used to obtain the mean velocity profiles both at the inflow, as well as the green points in Fig. 7. Since the hot wire is not sensitive to flow direction, a cone-shaped five-hole probe was used to study the local flow properties in more detail. The probe used is shown in Fig. 9. Due to the expected complex flow field between the buildings of the city model, e.g., large backwater areas, the probe needs to be able to handle a large range of flow direction angles. Hence, special care has to be taken during the calibration and use of the five-hole probe. In the experiment an aerodynamic alignment is first performed to completely cover 360 degrees for the yawing angle β. Essentially, this means that the probe was turned about its jawing axis until $p_2 \approx p_3$. This angular position is recorded and later added to the flow angle determined by the probe.

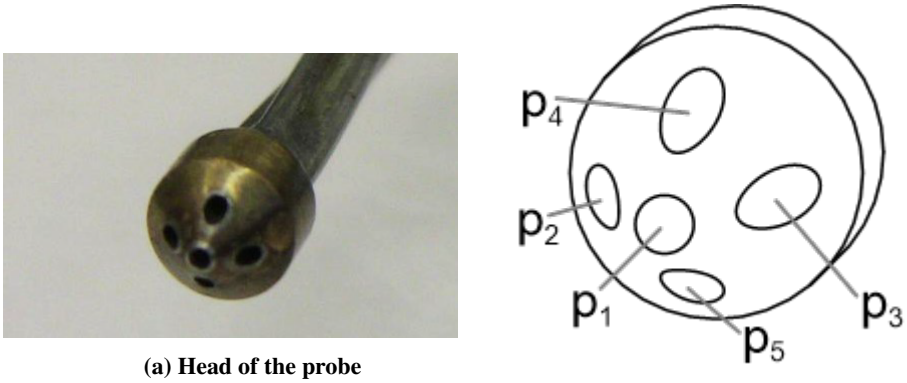

(a) Head of the probe **(b) Schematic view**

Fig. 9 Cone-shaped five-hole probe.

The probe was calibrated in a separate facility on a traverse system where it could be rotated about its angle of attack and yawing axes. Calibration was carried out for angles of attack from -62.5 to +75 degrees in steps of 2.5 degrees and for yawing angles from -30 to +30 degrees in steps of 2, 3 and 5 degrees. In total 1232 calibration points were recorded. A novel calibration method based on the ideas proposed in [9] or [10] is used for the calibration of the five-hole probe. It follows a five-zone approach for the mathematical formulation of the calibration function for large angles. To cover a wide range of flow angles, the calibration function is divided into five different functions each covering a distinct flow direction. Specifically the following five zones are defined: small angles, large positive and negative angles of attack,

and large positive and negative yawing angles. Each zone is characterized by the position of the maximum pressure, e.g. the small angle zone is the zone where p_1 is the largest pressure, or the large positive angle of attack zone is where p_5 is the largest pressure. This division in zones allows eliminating the pressure measurement from the opposite side where the flow is separated during the calibration. In other word p_4 is not considered for large angle of attack.

The five calibration functions (one for each zone) are chosen based on [11]. They use a reference pressure which is the sum of the pressure differences, e.g. $p_{ref} = 4p_1 - p_2 - p_3 - p_4 - p_5$ for small angles or $p_{ref} = 3p_5 - p_1 - p_2 - p_3$ for large angle of attack. As basis for the following polynomial fitting the functions X and Y are selected as the relative difference pressure of the two opposing holes with respect to the reference pressure, i.e. $X = \frac{p_4 - p_5}{p_{ref}}$ and $Y = \frac{p_2 - p_3}{p_{ref}}$ for small angles, respectively. In this approach, the dynamic pressure is eliminated and the parameters are only dependent from the flow angles as long as fluid mechanical similarity can be assumed. The dependency the flow angles from X and Y is approximated by polynomial functions within each zone in accordance to the following equations.

$$\begin{aligned} \alpha &= \sum_{i=0}^{5} \sum_{j=0}^{4} A_{i,j} X^i Y^j \\ \beta &= \sum_{i=0}^{5} \sum_{j=0}^{4} B_{i,j} Y^i X^j \\ q &= p_{ref} \sum_{i=0}^{4} \sum_{j=0}^{4} Q_{i,j} Y^i X^j \\ p &= \max_k(p_k) - p_{ref} \sum_{i=0}^{4} \sum_{j=0}^{4} P_{i,j} Y^i X^j, \end{aligned} \tag{1}$$

where A, B, Q, and P are the coefficient matrices which are fitted in the calibration.

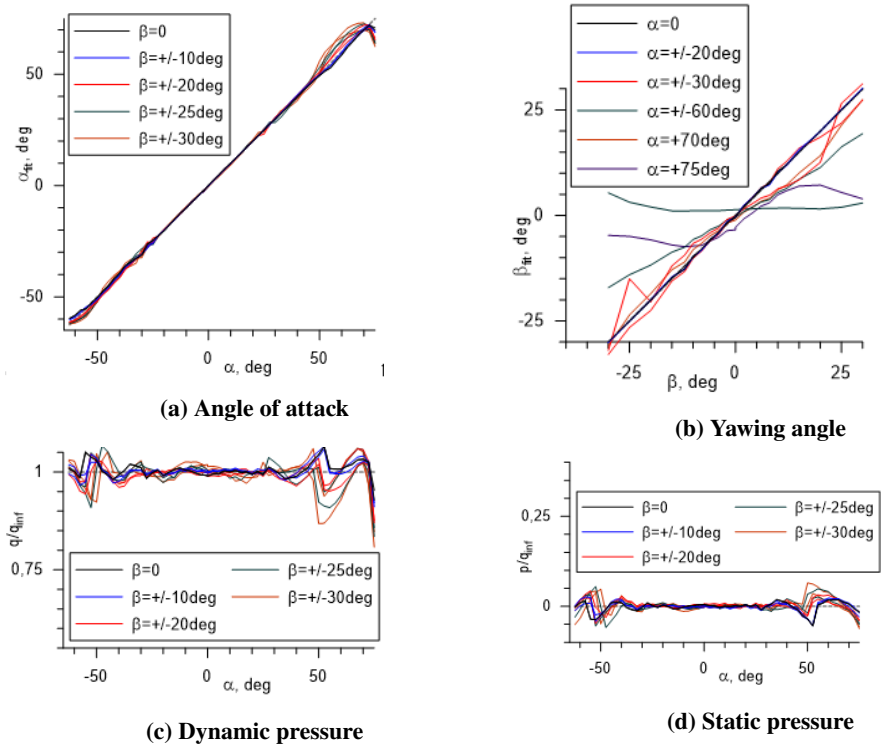

(a) Angle of attack

(b) Yawing angle

(c) Dynamic pressure

(d) Static pressure

Fig. 10 Representation of the calibration data by the fitting functions.

The results of the calibration are shown in Fig. 10. The angle of attack can be determined reliably up to about 70 degrees, see Fig. 10a. On the other hand, the yawing angle determination becomes difficult for high angles of

attack since the pressure difference $p_2 - p_3$, or its sensitivity to the yawing angle, shows quite an oscillating behaviour that cannot be covered by the chosen approach (Fig. 10b). Higher order fitting functions would require a lot more supporting points and significantly increase calibration effort. The fitting functions for dynamic and static show a similarly oscillating behaviour for combinations of high angles of attack and yaw (Fig. 10c and 10d).

Due to the nonlinear characteristics of the calibration function, the time averaged flow properties may differ significantly from those calculated from the time averaged pressures. For this reason, the mean flow properties shown later are calculated separately for every time instant and averaged afterwards. Finally, note that the probe was installed with short connections to the pressure transducers to enable resolution of unsteady flow phenomena. The measurements have been conducted with a sampling frequency of 1000 Hz and an averaging time of 20 s.

IV. Results and Comparison to Large Eddy Simulation

A. Inflow Velocity Profile

Fig. 11 shows both the profile of the scaled wind tunnel experiment and the LES simulation, normalized to u_{REF}, the velocity u at the height of z_{REF} =30 m. The free stream velocity is 6.5 m/s in the simulation and 25 m/s in the experiment. Due to the length scale of 1:100, Reynolds numbers are about factor 25 higher in the simulation. Because of the sharp edged buildings a good agreement could be achieved in the area of the building height. As will be later shown with the hot wire probe and the five-hole probe, the flow is essentially Reynolds number independent. Remarkable deviations only occur above 50 m. These are outside the considered altitude range.

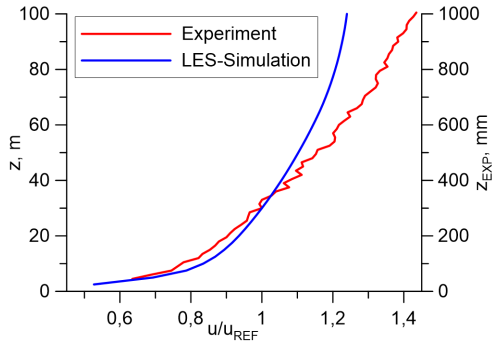

Fig. 11 Inflow velocity profile close to the wind tunnel nozzle compared to LES-simulation.

B. Flow Properties on the Ground

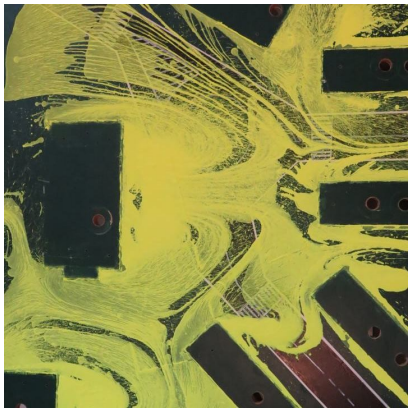

Fig. 12 Oil-flow-visualization showing the backwater area downstream of the third high-rise building.

In order to identify distinctive flow structures in the wake of the buildings, oil-flow-visualization tests were carried

out for the assumed wind direction with the three high-rise buildings upstream. The most informative structures are represented by the traces of paint on the floor which manifest a footprint of the flow between the buildings, as shown in Fig. 12. The flow direction in the image is from the left with an free stream velocity of 25 m/s. The wakes of the high-rise buildings are particularly clear where vortices from both sides collapse. Furthermore, a channeling of the flow between the terraced houses can be observed.

Fig. 13 shows the results of the wall shear probes. For better visibility, the results of the 37 probes located at the positions defined in Fig. 7 are interpolated to generate coloured areas. The results are further given in terms of $\sqrt{\Delta c_p}$. This offers a better comparability to the velocities measured later on with hot wire and five-hole probe. The results in Fig. 13 compare well to the oil-flow images. The greatest local acceleration is visible between the northernmost high-rise building and the supermarket. The area behind the southernmost high-rise building is characterized by wake effects from all three high-risers, which makes it a very complex flow structure. The negative values in $\sqrt{\Delta c_p}$ could potentially be the result of large vertical flow velocities.

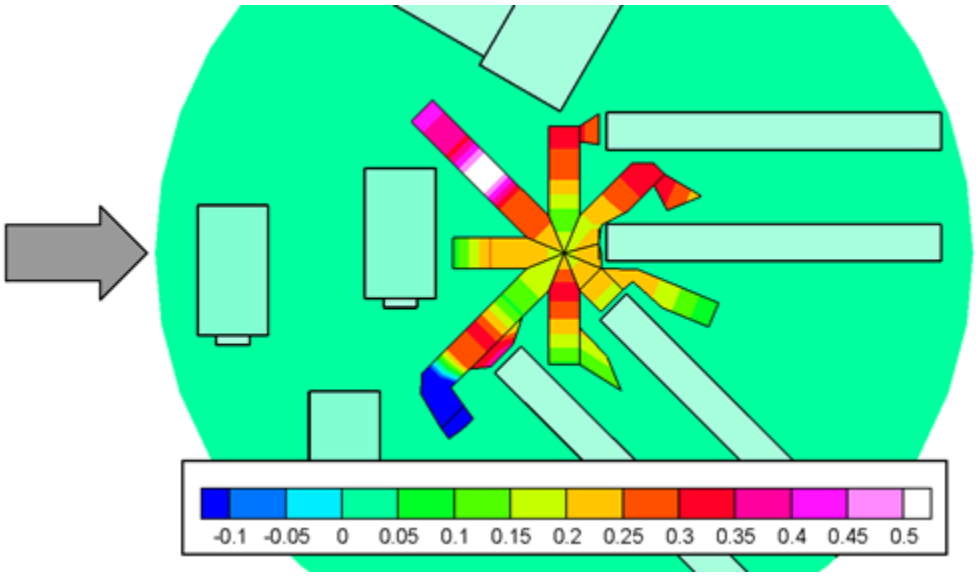

Fig. 13 Results of the wall shear probes in the floor measured by $\sqrt{\Delta c_p}$.

C. Velocity Profiles along the Flight Path

1. Five-hole probe measurements

Velocity profiles were measured using the five-hole probe for the green positions 2, 3, and 4 along the flight path in Fig. 7. The experiment was run at four different wind speeds: 16, 21, 27, and 32 m/s. Fig. 14 shows time averaged flow angles and local velocities versus the vertical position. Recall that the numerical simulation used the full scale city model and a free stream velocity of 6.5 m/s. It shall be noted that in lower altitude regions between buildings the five-hole probe measured pressure combinations which did not produce meaningful results with the chosen calibration function. These outliers have been removed from the presented results. A first noticeable result is that the experiment shows no Reynolds number dependence. It can be assumed that this independence of the Reynolds number carries over to the higher numbers at full scale from the numerical simulation. In comparison to the LES results, at a first glance, there are significant deviation noticeable. This difference is not surprising considering the relatively coarse spacing in the LES mesh (2.5 m). Hence, the positions are not exactly the same in a region of very strong gradients. Furthermore, on the experiment, the flow is always influenced by the probe. This effect is not covered by the calibration when the probe moves close to surfaces. Finally, the flow structures are very complex which makes deviations between experiment and simulation more likely. Still, focusing on the effects of the buildings on the flow field, a similar flow structure can be recognized within both numerical simulation and experimental results.

First looking at Position 2, which is situated directly in front of a 20 m tall terraced house, both experiment and LES identify an flow acceleration and an equally strong upwind component (increased angle of attack) at the upper edge of

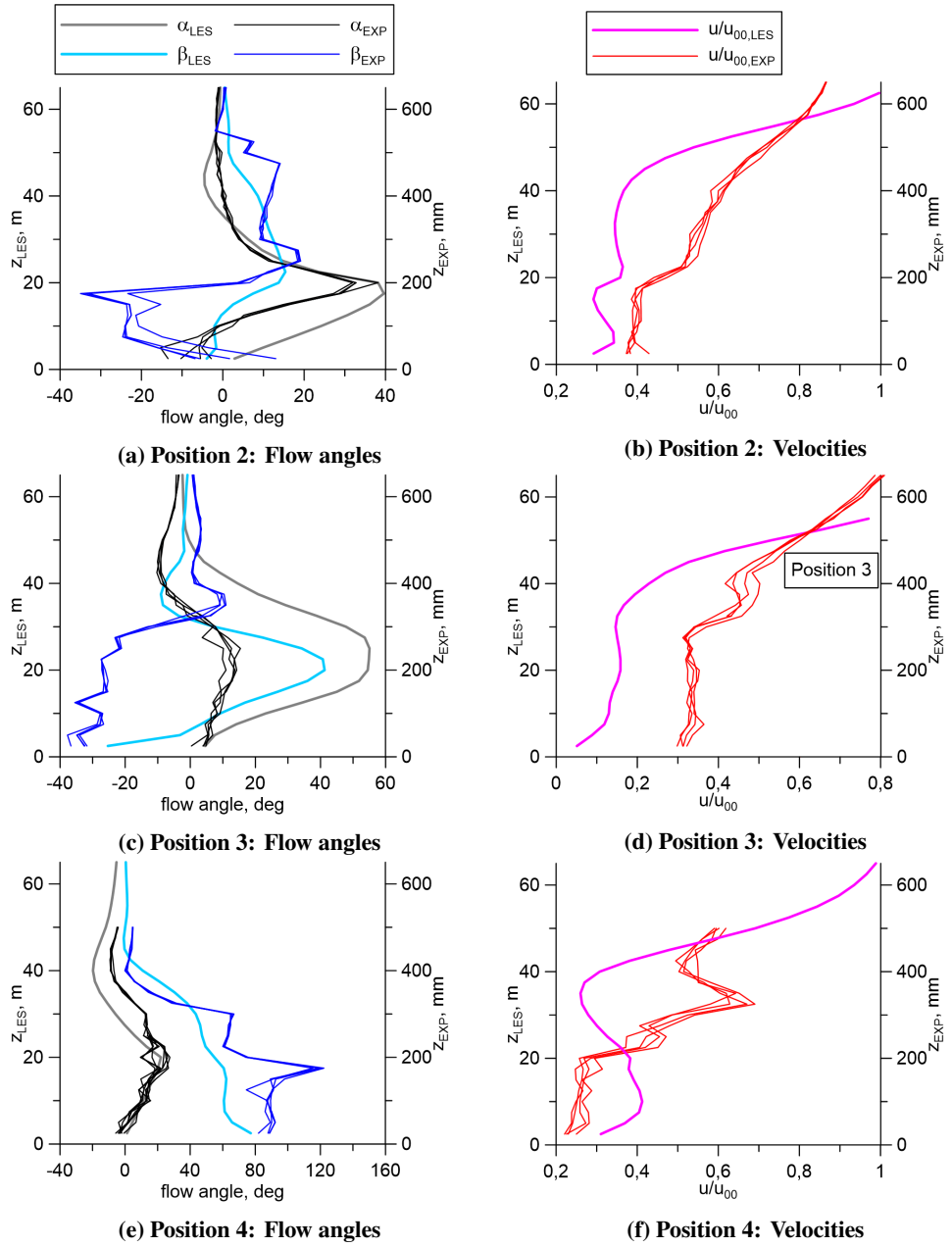

(a) Position 2: Flow angles

(b) Position 2: Velocities

(c) Position 3: Flow angles

(d) Position 3: Velocities

(e) Position 4: Flow angles

(f) Position 4: Velocities

Fig. 14 Velocity profiles measured with five-hole probe in comparison to LES results.

the building. At the same time, the horizontal wind direction does not behave as predicted. Moreover, the wake of the high rise building upstream of Position 2 is predicted to too strong in the LES resulting in a much lower velocity between 20 and 50 m height in comparison to the experiment.

The strongest deviations between simulation and experiment can be observed at Position 3. At this point, the flow fields around three buildings interact with each other: The wake of the high-rise building in the west and the flow around the corners of two terrace houses, the latter forming some kind of nozzle for the flow close on the ground (see Fig. 7). As can be estimated from the mean velocity, the high building's wake may be predicted too strong again in the LES, resulting in a wind deflection to the opposite direction and an upwind angle that is four times too high.

At Position 4, the flow directions show the best agreement between LES and wind tunnel, even though it is right in front of a building's surface facing directly upstream. Note that the flow in Position 4 should be most sensitive to small variations which could lead to severe directional changes. In the experiment the flow acceleration at the upper

edge of the downstream building is again clearly present. However, this effect is completely missing in the numerical data. Instead the effect seems to disappear completely in the wake of the high building upstream, whose strength is consistently overestimated at all positions.

In addition to the averaged results shown in Fig. 14, the time history of the measurements at Position 2 and Position 3 are presented in Fig. 15 and Fig. 16, respectively. Both measurements have been taken at a free stream velocity of 27 m/s at a height of 200 mm in the experiment. The sampling rate of the data was 1000Hz as previously specified in Section III. The time interval shown in the figures is 1000 ms. Note that because of the scales in length and velocities, the time scale in real life is between two and three orders of magnitude longer than in the wind tunnel. In other words the 1000 ms wind tunnel data is representative of several minutes of real life data. Both figures depict a highly unsteady flow with a broad variation of flow angles. There is a strong correlation between extrema in flow angles and extrema in dynamic and static pressure.

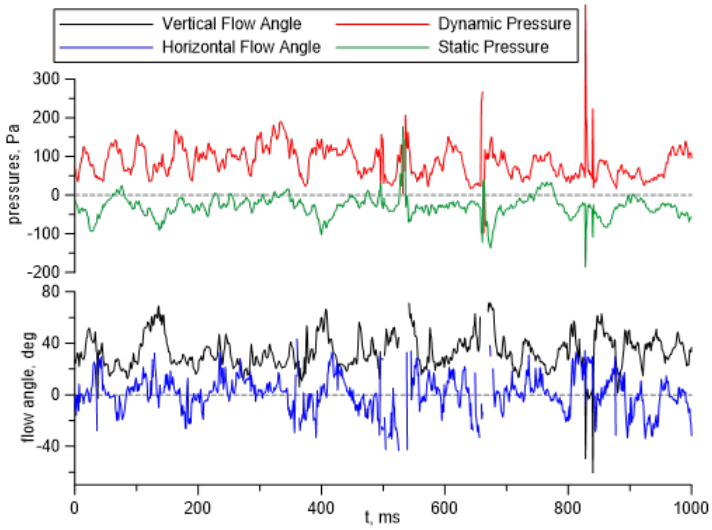

Fig. 15 Angle and pressure time history for u_∞=27 m/s (q_∞=440 m/s) at Position 2 and z_{EXP}=200 mm.

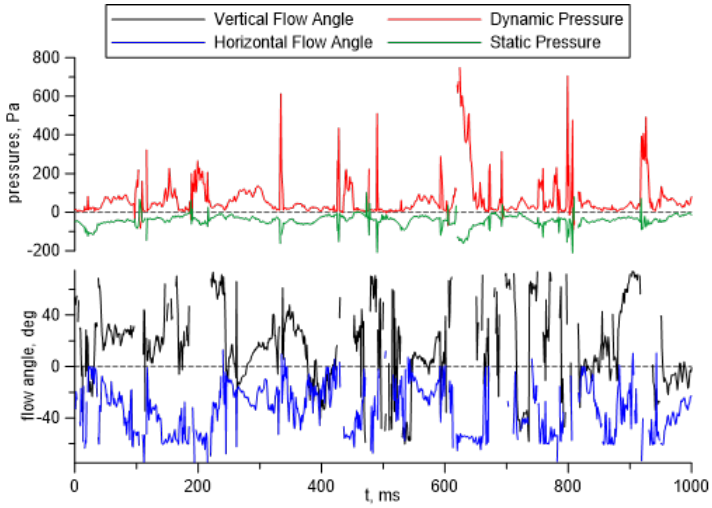

Fig. 16 Angle and pressure time history for u_∞=27 m/s (q_∞=440 m/s) at Position 3 and z_{EXP}=200 mm.

Comparing the time histories with the averaged results gives an indication of how unsteady the flow is at Position 2 and 3. For example, the mean upwind angle at Position 2 at z_{EXP}=200 mm in both LES and experiment is more than 30 degrees, see Fig. 14a. However, the time series between 800 and 850 ms in Fig. 15 shows two downwind events with

angles down to -45 degrees in combination with gust velocities up to 30 m/s. While in the wind tunnel these events only lasted a few milliseconds, they would represent time periods of several seconds in real life.

Similar observations can be made at Position 3 (Fig. 16). The LES predicts mean upwind angles of more than 50 degrees at z_{EXP}=200 mm at this position. The wind tunnel experiment still results in mean upwind angles between 11 and 14 degrees, see Fig. 14c. The time series in Fig. 16 on the other hand shows multiple events with temporary downwind angles down to -45 degrees. At the same time the measurements indicate gust velocities up to 35 m/s.

2. Hot wire measurements

Velocity profiles have been obtained using a single hot wire at five positions (green points) along the flight path, see Fig. 7. Three different wind speeds have been tested in the experiment, namely 16 m/s, 20 m/s and 24 m/s. The results of the measurements compared to the LES data is shown in Fig. 17. Here, the velocity is only the horizontal component, which is the component measured by the vertically aligned hot wire. In general, the hot wire measurement shows good agreement with the five-hole probe measurements. The Reynolds number independence is again clearly visible, as is the flow acceleration over the upper edge of the downstream building in Position 2.

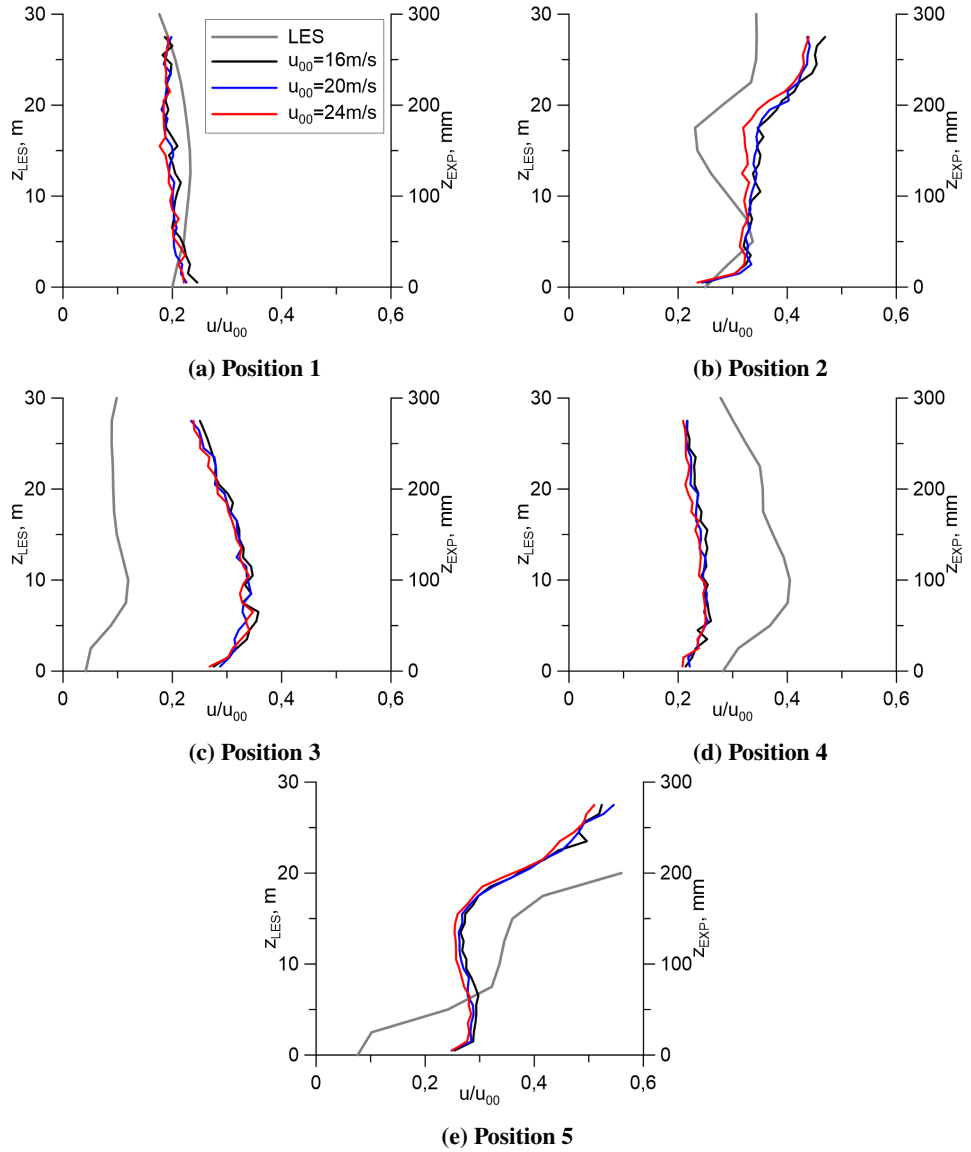

Fig. 17 Velocity profiles measured with hot wire in comparison to LES results.

V. Conclusion

The wind field through a realistic city model representing a typical European urban area was studied in a wind tunnel experiment. The experimental results are used to validate previous numerical studies based on the LES-tool PALM, which built the basis for a flight path optimization in a UAV delivery scenario. The results show quite good consistency for the atmospheric boundary layer profile in the inflow. However, the results between the buildings can differ largely from numerical simulation to experimental work. This warrants further investigation.

The wind field close to surface was studied with oil-flow visualization and pressure probes in the ground. Additionally, at representative points spread over the city model, the velocity and flow angle profiles over altitude were obtained with hot wire anemometry and a five-hole pressure probe, respectively. In order to measure flow angles over a wide range, a five-zone approach together with aerodynamic alignment was applied. By keeping the connections from probe to pressure transducers as short as possible, a satisfactory time resolution could be achieved. Information about turbulence and gustiness was gathered. It shall be noted that the approach still fails to find an aerodynamic alignment at high turbulence levels. The rapid changes in flow direction produce too many outliers that are not within the range of the calibration function.

In conclusion, particular attention has to be paid to unsteady flow phenomena such as gusts and turbulence. In the context of UAV flight path planning, this means that in addition to the mean wind field, areas of unsteady flow need to be identified and avoided during flight. For instance, adequate clearance should be kept from building edges, even if strong upwind is predicted which could improve the energy efficiency of the UAV.

Acknowledgments

This research was funded by the German Federal Ministry for Economic Affairs and Climate Action under grant number 20D2106C. The responsibility for the content of this paper is with its authors. The financial support is gratefully acknowledged.

References

[1] Kirschstein, T., "Comparison of energy demands of drone-based and ground-based parcel delivery services," *Transportation Research Part D: Transport and Environment*, Vol. 78, 2020, p. 102209.

[2] Rienecker, H., Hildebrand, V., and Pfifer, H., "Energy optimal flight path planing for unmanned aerial vehicle in urban environments," *CEAS EuroGNC*, 2022.

[3] Rienecker, H., Hildebrand, V., and Pfifer, H., "Energy optimal 3D flight path planning for unmanned aerial vehicle in urban environments," *CEAS Aeronautical Journal*, 2023, pp. 1–16.

[4] Rienecker, H., Hildebrand, V., and Pfifer, H., "Energy Optimal Flight Path Planning for Unmanned Aerial Vehicles in Urban Environments Based on a Novel Energy-Distance Map," *SciTech*, 2024.

[5] Maronga, B., Gryschka, M., Heinze, R., Hoffmann, F., Kanani-Sühring, F., Keck, M., Ketelsen, K., Letzel, M. O., Sühring, M., and Raasch, S., "The Parallelized Large-Eddy Simulation Model (PALM) version 4.0 for atmospheric and oceanic flows: model formulation, recent developments, and future perspectives," *Geoscientific Model Development*, Vol. 8, No. 8, 2015, pp. 2515–2551.

[6] VDI Verein Deutcher Ingenieure, "Physical Modelling of Flow and Dispersion Processes in the Atmospheric Boundary Layer—Application of Wind Tunnels," *VDI Verein Deutcher Ingenieure, Düsseldorf*, 2000.

[7] Franke, J., Hellsten, A., Schlünzen, H., and Carissimo, B., "Best practice guideline for the CFD simulation of flows in the urban environment," Ph.D. thesis, COST European Cooperation in Science and Technology, 2007.

[8] King, L., "On the Convective Heat Transfer from Small Cylinders in a Stream Of Fluid. Determination of Convective Constants of Small Platinum Wires with Application to Hot-Wire anemometry," *Phil. Trans. R. SOC. A*, Vol. 214, 1914, pp. 373–432.

[9] Paul, A. R., Upadhyay, R. R., and Jain, A., "A novel calibration algorithm for five-hole pressure probe," *International Journal of Engineering, Science and Technology*, Vol. 3, No. 2, 2011.

[10] Zilliac, G., "Modelling, calibration, and error analysis of seven-hole pressure probes," *Experiments in Fluids*, Vol. 14, No. 1-2, 1993, pp. 104–120.

[11] Treaster, A. L., and Yocum, A. M., "The calibration and application of five-hole probes," *24th International Instrumentation Symposium*, 1978, pp. 255–266.